Available online at www.sciencedirect.com

SCIENCE DIRECT

Biochimica et Biophysica Acta 1667 (2004) 67–81

BIOCHIMICA ET BIOPHYSICA ACTA
BBA

http://www.elsevier.com/locate/bba

The interactions of the HIV gp41 fusion peptides with zwitterionic membrane mimics determined by NMR spectroscopy

Kevin F. Morris[a,b], Xinfeng Gao[c], Tuck C. Wong[a,*]

[a]*Department of Chemistry, University of Missouri, Columbia, MO 65211, United States*
[b]*Department of Chemistry, Carthage College, Kenosha, WI 53140, United States*
[c]*Department of Chemistry, Indiana University, Bloomington, IN 47405, United States*

Received 23 June 2004; received in revised form 25 August 2004; accepted 31 August 2004
Available online 17 September 2004

Abstract

The wild-type (wt) N-terminal 23-residue fusion peptide (FP) of the human immunodeficiency virus (HIV) fusion protein gp41 and its V2E mutant have been studied by nuclear magnetic resonance (NMR) spectroscopy in dodecylphosphocholine (DPC) micelles as membrane mimics. A number of NMR techniques have been used. Pulsed field-gradient diffusion measurements in DPC and in 4:1 DPC/sodium dodecylsulfate mixed micelles showed that there is no major difference between the partition coefficients of the fusogenic wt peptide and the V2E mutant in these micelles, indicating that there is no correlation between the activity of the fusion peptides and their membrane affinities. The nuclear Overhauser enhancement (NOE) patterns and the chemical shift index for these two peptides indicated that both FP are in an α helical conformation between the Ile^4 to Leu^{12} or to Ala^{15} region. Simulated annealing showed that the helical region extends from Ile^4 to Met^{19}. The two FPs share similar conformational characteristics, indicating that the conformation of the FP is not an important factor determining its activity. The spin-label studies, utilizing spin labels 5- and 16-doxystearic acids in the DPC micelles, provided clear indication that the wt FP inserts its N-terminus into the micelles while the V2E mutant does not insert into the micelles. The conclusion from the spin-label results is corroborated by deuterium amide proton exchange experiments. The correlation between the oblique insertion of the FP and its fusogenic activity is in excellent agreement with results from our molecular dynamics simulation and from other previous studies.

Keywords: HIV; Fusion peptide; Membrane fusion; NMR; Spin-label; Membrane binding

1. Introduction

Enveloped viruses such as human immunodeficiency virus (HIV) and influenza virus infect their target cells by cell-specific binding to the cell membrane followed by the fusion of the viral enveloped membrane with the membranes of the target cells [1]. Usually only one viral protein is responsible for the actual membrane fusion step. For many viruses, a segment usually located at the N-terminus of the fusion protein is responsible for the initial stage in the membrane fusion process [2]. This segment is generally referred to as the fusion domain or fusion peptide (FP). The interaction of the FP with membranes has many membrane perturbing properties [3] and accelerates the rate of liposome fusion in model membrane systems. The HIV-1 fusion protein, glycoprotein gp160, contains two non-covalently associated subunits, gp120 and gp41 [1]. The subunit gp120 is responsible for viral binding to CD4 [4] and chemokine receptors [5–7] on the membrane surface of the target cells, while the transmembrane subunit, gp41, is responsible for the initiation of the membrane fusion process [8]. The N-terminal 16 residues of the gp41 fusion domain (AVGIGALFLGFLGAAG) are mostly hydrophobic, while the extended domain consisting of 23 or 33 residues contains more polar residues. The FP is highly homologous with corresponding domains of other enveloped viruses [9]. An absolutely conserved five-residue FLGFL sequence at positions 8–12 is a prominent motif among the HIV family, and was proposed to be essential in fusogenic activities [10].

* Corresponding author. Tel.: +1 573 8827725; fax: +1 573 8822754.
E-mail address: wongt@Missouri.edu (T.C. Wong).

0005-2736/$ - see front matter © 2004 Elsevier B.V. All rights reserved.
doi:10.1016/j.bbamem.2004.08.014

Mutagenesis studies of intact enveloped proteins as well as the synthetic FP's strongly implicated the role of the FP domain in mediating membrane fusion [11–13]. Mutations with a polar residue in this domain either in intact gp41 fusion protein or in synthetic peptides, such as V2E and L9R, reduce the fusogenic activities drastically [12–16]. The fusion domains of HIV-1 and many other enveloped viruses such as HIV-2, SIV and influenza contain an unusually large number of glycine residues. When the glycines at position 10 and 13 in the absolutely conserved FLGFLG motif are mutated, the activity was found to be completely eliminated. Mutations of the glycines at position 3 and 5 reduce but do not eliminate the activity of the fusion peptide [13].

Polarized attenuated total reflection infrared spectroscopy (ATR-IR) has been used to determine the orientation of fusion peptides with respect to the membrane surface [17,18]. It was suggested that, based on the correlation of the tilt angle of the inserted FP with respect to the membrane interface and the fusogenic activity of the FP, the oblique insertion of the viral FP is required for fusogenic activities. Inactive FP mutants orient parallel or more parallel (than the wt FP) to the membrane surface instead. Results from nuclear magnetic resonance (NMR) [19] and ESR power saturation techniques [20,21] for the influenza hemagglutinin HA_2 FP also reached such a conclusion.

To date, only a few modeling/simulation studies on the interaction of viral fusion peptides with membrane have been carried out. Hydrophobic moments and hydrophobic index have been used to estimate the interaction of the HIV and other FP's with membrane [22,23]. Recently, we reported the first all-atom MD simulation study of the HIV-1 FP in an explicit palmitoyloleoyl-phosphatidylethanolamine (POPE) lipid bilayer, in which the wild-type FP, its V2E and L9R mutants and a shortened peptide consisting of the 5–16 segment were studied. The results showed that the active wt peptide is inserted obliquely into the bilayer ($44\pm6^\circ$ with respect to the bilayer normal), while the inactive mutants and fragment bind to the surface of the bilayer and lie parallel to the bilayer surface (90°) [24]. Furthermore, the inserted wt FP perturbed the bilayer by increasing the length of the interfacial area, while the surface-bound mutants do not. Thus, it demonstrated that MD in explicit membrane model can produce results that are consistent with experiments and provide molecular interpretation of processes that may be inaccessible experimentally. The MD results are in excellent agreement with the hypothesis that in order for the FP to be active, it must be inserted into the bilayer in an oblique angle [18,25]. Subsequently, Maddox and Longo [26], using Monte-Carlo simulation and simplified models for the FP and the lipid bilayer, studied the binding of the gp41 FP and several of its mutants and concluded that the diminished activity of the mutants is due to "their partitioning into unfavorable (surface-adsorbed) conformations". Another all-atom MD study from this laboratory examined the role of the abundant and conserved glycine residues in the fusion domain [27] and found that conformational flexibility at the glycine sites (G5, G10 and G13) is correlated with fusogenic activity. Active FPs exhibit conformational flexibility at one of the glycine sites while inactive FPs do not such possess conformational flexibilities.

In this work, the active wild-type (wt) (AVGIGALFLGFLGAAGSTMGARS.NH_2) and an V2E mutant (AEGIGALFLGFLGAAGSTMGARS.NH_2) of the 23-residue fusion peptide of the HIV-1 gp41 protein) were studied by NMR spectroscopy in dodecylphosphocholine (DPC) micelles. The wt FP is identical to the N-terminal sequence of the LAV_{1a} strain [28]. The goals of this work are to address the questions of how the conformation of the FPs, their membrane affinity and their mode of binding to the membrane are correlated with their fusogenic activities, and to compare with the MD simulation of these two, and other, FPs in lipid bilayers [24]. Previous NMR studies of the wt FP have been made in SDS micelles [29,30] and in phosphatidylcholine vesicles [31]. The F8Y mutant was also studied in the SDS micelles by Chang et al. [29]. Several solid state NMR studies of the FP [32,33] and its cross-linked form [34] in lipid bilayers have also been made.

2. Experimental procedures

2.1. Samples

The wt and V2E fusion peptides were synthesized in the Peptide Synthesis Facility at the Department of Chemistry of the University of Missouri. All peptides were purified by HPLC and were of >95% purity. The identity of the peptides was checked by mass spectrometry. Perdeuterated lipids DPC-d_{38} and SDS-d_{23} were purchased from Cambridge Isotopes (Andover, MA). The aqueous samples for diffusion measurements contained 0.5 mM of peptides in 90% H_2O/10% D_2O. A typical micellar sample was made of 2 mg of peptide in 0.5 ml of ~90 mM DPC-d_{38} in 90% H_2O/10% D_2O in a 5-mm NMR tube, corresponding to ~2 mM in peptide concentration. The pH of all samples was adjusted to ~7 by adding small amounts of HCl or NaOH.

In some samples 20 mol% (of total lipid) of SDS-d_{23} was added to DPC to make zwitterionic/anionic mixed micelles (see discussion in Results). The total concentration of the lipids in these sample was ~110 mM.

2.2. Spin label studies

For experiments using spin-labels (SL), two spin labels, 5-doxystearic acid (5-DS) and 16-doxystearic acid (16-DS), obtained from Aldrich, were used. Stock solutions of 5-DS and 16-DS of ca. 0.1 mM were made by dissolving 5.2 mg of 5-DS and 4.9 mg of 16-DS in 1 mL of methanol-d_4, respectively. Seventy microliters of the stock solution of each SL sample was taken from the stock solution and was allowed to evaporate to dryness in a vial. Then ~0.6 mL of

FP/DPC sample was then added to the vial to redissolve the SL. In both cases, the SL was added in a mole ratio of ~1:65 SL:DPC. That is less than one SL per micelle (the aggregation number for DPC micelles is ~56) [35].

2.3. NMR spectroscopy

All NMR experiments were performed on a Bruker DRX-500 MHz or a Varian Inova 600 MHz spectrometer. For most of the samples, the following experiments were done: one-dimensional ^{1}H spectra, TOCSY spectra [36,37] and NOESY spectra [38,39]. The typical experimental conditions for all two-dimensional NMR experiments were as follows. DRX-500: the ^{1}H 90° pulse was about 8 μs. All experiments were obtained in the phase-sensitive mode by using the TPPI method [40]. Typically, 16–32 scans per t_1 was acquired in 512×2K data sets which were then zero-filled to 1K×2K after Fourier transform in both dimensions. $\pi/3$ shifted sine-bell squared apodization was used in both dimensions. Water suppression was achieved by using WATERGATE [41] in all 2D experiments. In 1D experiments, either WATERGATE or low-power presaturation was used. The TOCSY mixing time is 80 ms.

For the Varian Inova 600-MHz spectrometer, the pulse width was ~7 μs and the spectral width 8000 Hz. The States-TPPI method was used for all 2D experiments. 512×4K data sets were acquired and zero-filled to 1K×2K. The data sets were then converted and processed by the Bruker Xwinnmr software as described earlier.

Experiments were performed at two temperatures, 298 and 310 K. The temperature was controlled by passing dried-air to the probe through a Haake constant-temperature bath. The stability of the temperature control was ~0.1 K.

The pulsed-field-gradient (PFG) LED pulse sequence [42] was used for diffusion experiments. Low-power presaturation was used preceding the pulse sequence to suppress the water signal. The diffusion time, Δ, was 56 ms, the gradient duration, δ, 5 ms and the relaxation delay 10 s. 16–32 scans were obtained for each spectrum. PFG was applied in both the x and y directions for micellar samples and only in the x direction for aqueous samples. The gradient strength in a series of experiments was typically incremented from 0.5 to ~50 G/cm in 10–13 steps. All diffusion experiments were performed on the Bruker DRX-500 spectrometer equipped with a three-axis Accustar gradient driver. The detailed procedure for the determination of the diffusion coefficients and the partition coefficients of peptides in micelles by NMR PFG diffusion techniques was described in two previous papers [43,44]. Briefly, the bound fraction of the peptide, f_b, is determined from

$$f_b = (D_f - D_{obs})/(D_f - D_b)$$

where D_f and D_b denote the diffusion coefficients of the peptide in the free and bound states, respectively; D_{obs} is the experimentally observed diffusion coefficient of the peptide in the presence of the micelles. Because the root mean square displacement of the peptide during the diffusion time allowed in the experiment (typically ~50 ms) is much larger than the dimension of the micelles, D_b can be taken as equal to the diffusion coefficient of the micelles, D_{micl}. The partition coefficient is then calculated according to the definition of Tamm [45].

In deuterium exchange experiments, the FP/DPC samples were lyophilized several times in H_2O, and then D_2O was added to the freeze-dried sample. The 1D experiments were conducted at 293 K immediately after the dissolution of the sample in D_2O. The earliest time a spectrum was taken is about 5 min after the sample was prepared.

2.4. ESR spectroscopy

The ESR experiments were done on a Bruker ESP300 spectrometer at ~298 K with the following parameters: microwave power: 10 mW; center field: 3360 G; sweep width: 100 G; sweep time: 168 s; time constant: 328 ms; modulation amplitude: 5 G; and modulation frequency: 100 KHz. The samples for the ESR experiment were similar to those for the NMR experiments in the SL and DPC concentrations. Three levels of FP amounts were used for each case, no FP, 0.5 mg FP (~1.2 mM) and 1.0 mg FP (~2.4 mM), respectively.

2.5. Structural calculations

Structures were calculated using a simulated annealing protocol with the Discover [46] software, version 2.9.8 (Accelrys, San Diego, CA). The Consistent Valence Force Field (CVFF) was used. The nonbond cutoff was 12.0 Å, and the dielectric constant was 1. The van der Waals interactions were smoothly switched from 9.5 to 11.0 Å. Nuclear Overhauser enhancement (NOE) correlations observed in the NOESY spectra with 200 ms mixing time were used as distance constraints. According to the procedure of Wuthrich [47], distance constraints derived from sequential NOEs between backbone atoms (NH and αH) were classified into 2.7, 3.3, and 4.0 Å for strong, medium and weak NOEs, respectively. All other NOE distance constraints between residues more than one sequence position apart (medium range) were assigned to 4.0 Å if they involved exclusively backbone NH and αH, or to 5.0 Å if they involved side chain protons. The pseudo-atom correction was applied to NOE constraints involving equivalent or non-stereo-assigned protons [47]. A total of 90 (39 sequential and 51 medium range) and 94 (40 sequential and 54 medium range) distance constraints were used for the wt and V2E peptides, respectively.

The simulated annealing (SA) protocol used was similar to that reported by Nilges et al. [48]. A force constant of 30 kcal mol^{-1} Å^{-2} was used for NOE-derived distance constraints. The structure calculations were started with randomized atomic coordinates. An initial energy minimization with 500 steps of steepest descents was performed

with force constants of the covalent terms, quartic nonbound terms, and NOE terms reduced to 0.001 in their appropriate units. The minimized structure was heated to 1000 K in 0.5 ps. The NOE terms were gradually scaled to their full values during 16 ps dynamics at 1000 K. The covalent terms were scaled up more slowly during this period and reached their full values in another 4 ps of dynamics. The nonbound terms were kept at their initial low value during the first 16 ps of dynamics, and then gradually increased to their full values, which occurred after a total of 25 ps dynamics at 1000 K. The temperature was then cooled down to 300 K in the next 30 ps of dynamics. Finally, after the quartic nonbound terms were replaced by the Lennard–Jones form, the refined structure was minimized by 500 steps of steepest descents followed by conjugate gradients until a predefined convergence limit (<0.001 kcal $Å^{-1}$) was reached. During the entire simulation, a force of 50 kcal mol^{-1} rad^{-2} was used to force the ω angles to *trans* to prevent it from flipping to *cis* at high temperature.

3. Results and discussions

3.1. The secondary structure of the FPs in DPC micelles

Previous structural studies of the gp41 fusion peptide by NMR, IR, and CD techniques have yielded contradictory results. For example, CD measurements showed that the FPs have significant helical structure at low peptide/lipid (P/L) ratio (1:200) in SDS micelles [49,50] and in POPG vesicles [51]. NMR in SDS micelles and FTIR also indicate a helical structure in a significant region of the FP [29,52]. In contrast, at higher peptide/lipid ratio (1:10 in SDS micelles and 1:30 in POPG vesicles), there is significant β-strand character [50,51]. The β-strand structure was also confirmed by solid state NMR studies [32,33]. A study of the FP in phosphatidylcholine vesicles found that the α-helical content decreases with increasing P/L ratio, but still significant at a P/L ratio of 1:25 [31]. The present work provides information on the conformation of the FP and its V2E mutant in the environment of a neutral membrane mimic.

3.2. The wt-FP

Spectral and sequential assignments were carried out using the standard procedure of Wuthrich [47]. Spin systems were first identified from the TOCSY spectra and sequential assignments were then made from the NOESY connectivities. The chemical shifts of the wt-FP in DPC micelles at 298 K are given in Table 1a.

From the intramolecular NOE data derived from the NOESY cross-peaks, it can be shown that helical conformation prevails over the region from Val^2 to Ala^{21}. $d_{\alpha N}$ and $d_{\alpha\beta}$ of the (i, i+2), (i, i+3) and (i, i+4) types were observed in this region (Fig. 1). Contiguous $d_{NN}(i, i+1)$ were also present in this region, except for a couple with chemical shifts too close together for the cross peaks to be observed. A few $d_{NN}(i, i+2)$ and one $d_{NN}(i, i+3)$ were also present. However, the main α-helical

Table 1
Chemical shifts (in ppm from TSP) of the gp41 wt FP and its V2E mutant in 90 mM DPC micelles at 298 K

Residue	N-H	αH	βH	Others
a. *wt*				
Ala1		4.21	1.60	
Val2	8.81	4.29	2.21	γCH_3, 1.06
Gly3	8.60	4.13		
Ile4	8.86	3.96	2.01	γCH_2, 1.69, γCH_3, 1.03
Gly5	9.19	3.99, 3.80		
Ala6	8.21	4.18	1.54	
Leu7	8.11	4.18	1.95	γH, 1.70; δCH_3, 0.98
Phe8	8.51	4.40	3.32	
Leu9	8.60	4.09	1.97	γH, 1.65; δCH_3, 1.02
Gly10	8.30	3.98		
Phe11	8.16	4.49	3.32	
Leu12	8.24	3.95	1.79	γH, 1.57; δCH_3, 0.87
Gly13	8.17	3.94		
Ala14	8.00	4.37	1.53	
Ala15	8.35	4.17	1.37	
Gly16	8.45	3.99, 3.66		
Ser17	8.13	4.49	4.02	
Thr18	8.16	4.35	*	γCH_3, 1.32
Met19	8.20	4.47	2.18	γCH_2, 2.64, εCH_3, 2.13
Gly20	8.34	4.01		
Ala21	8.12	4.39	1.49	
Arg22	8.35	4.43	1.89, 1.77	γCH_2, 2.02; δCH_3, 3.29
Ser23	8.25	4.45	3.95	
b. *V2E*				
Ala1		4.19	1.69	
Glu2	8.87	4.45	2.16, 2.04	γCH_2, 2.43
Gly3	8.62	4.19		
Ile4	9.02	3.94	1.99	γCH_2, 1.68; γCH_3, 0.97
Gly5	9.18	3.96, 3.77		
Ala6	8.11	4.29	1.51	
Leu7	8.09	4.14	1.94	γH, 1.71; δCH_3, 0.95
Phe8	8.53	4.37	3.30	
Leu9	8.61	4.02	1.95	γH, 1.63; δCH_3, 0.99
Gly10	8.32	3.96		
Phe11	8.18	4.45	3.30	
Leu12	8.19	3.91	1.85	γH, 1.60; δCH_3, 0.85
Gly13	8.28	3.98		
Ala14	7.96	4.34	1.51	
Ala15	8.37	4.10	1.33	
Gly16	8.48	3.95, 3.88		
Ser17	8.11	4.50	4.01	
Thr18	8.16	4.32	*	γCH_3, 1.30
Met19	8.14	4.43	2.16	γCH_2, 2.62, 2.68, εCH_3, 2.12
Gly20	8.40	3.96		
Ala21	8.08	4.46	1.46	
Arg22	8.30	4.39	1.87, 1.76	γCH_2, 2.00; δCH_3, 3.27
Ser23	8.21	4.42	3.92	

* probably overlaps with the αH.

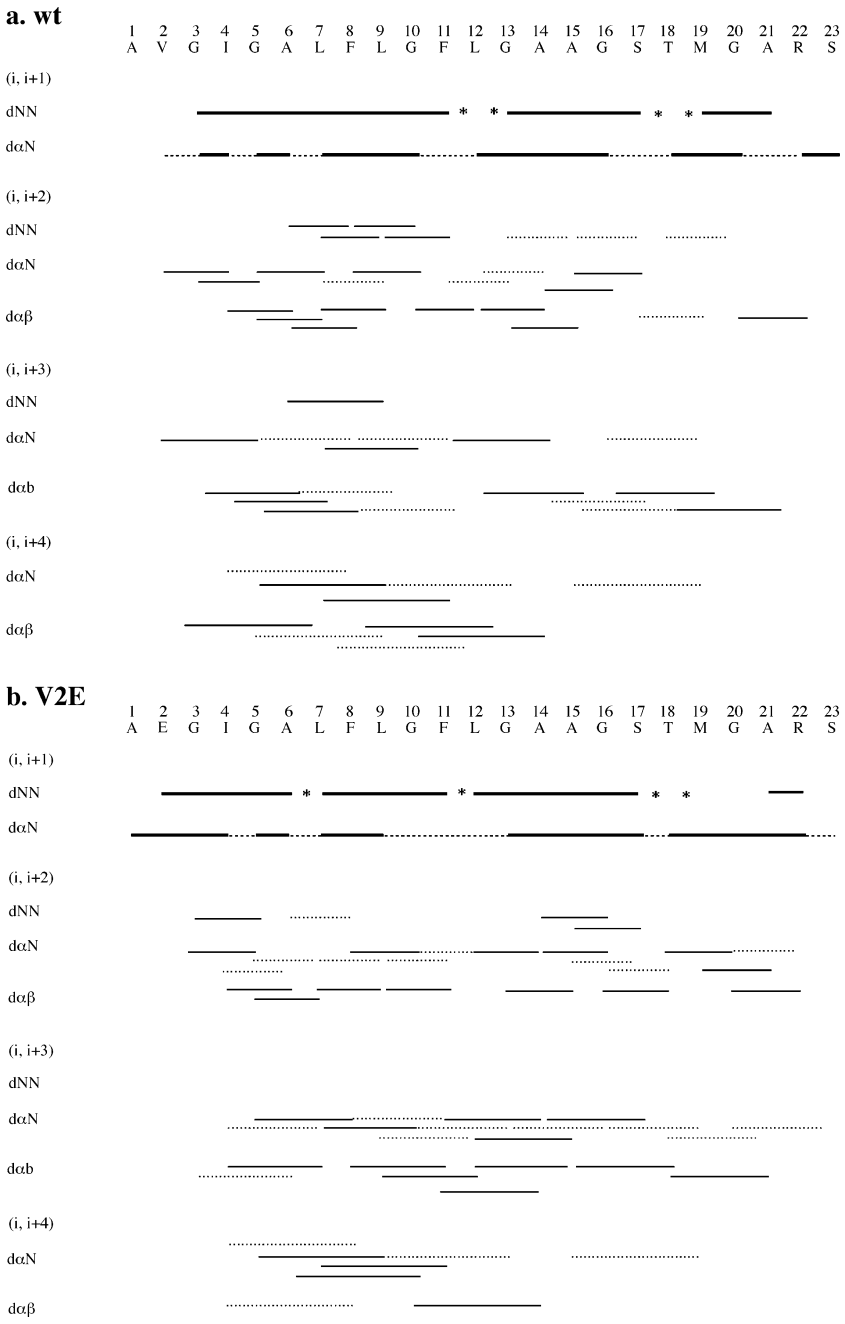

Fig. 1. The summary of NOE connectivity patterns for (a) wt FP and (b) the V2E mutant in DPC micelles obtained from combined results at 298 and 310 K. The thickness of the lines is approximately proportional to the intensity of the NOE cross-peaks. Broken lines represent ambiguous NOE correlations due to signal overlap. The asterisks in d_{NN} represent unobserved correlations due to the closeness of the NH chemical shifts involved.

region was found to lie between Val[2] and Leu[12], as $d_{\alpha N}(i, i+4)$ and $d_{\alpha\beta}(i, i+4)$ were observed only in this region. The $i, i+2$ connectivities in the 14–21 region may indicate a significant population of the nascent [53] or 3_{10} helices. The chemical shift index (CSI) or secondary chemical shifts [54] plots for the αH and βH (Fig. 2) also yield the same conclusion on the conformation of the peptides as reached from NOE. The αH shifts are consistently downfield from the respective random coil values in the Ile[4]–Ala[15] region (broken at Gly[10] and Gly[13]), while those of the βH are upfield from the random coil value, indicating helical structure in this region. The main region of significant downfield shifts for the αH occurs in the Ile[4]–Leu[12] or from the Ile[4]–Ala[15] region, indicating the α-helical structure in this segment, in agreement with the NOE data which showed that $(i, i+3)$ and $(i, i+4)$ NOE correlations are primarily present in the Ile[4]–Leu[12] region. The type I turn structure in the Thr[18] to Gly[20] segment as suggested by Chang et al. [29] in SDS micelles is not evident from the observed NOEs in the present data.

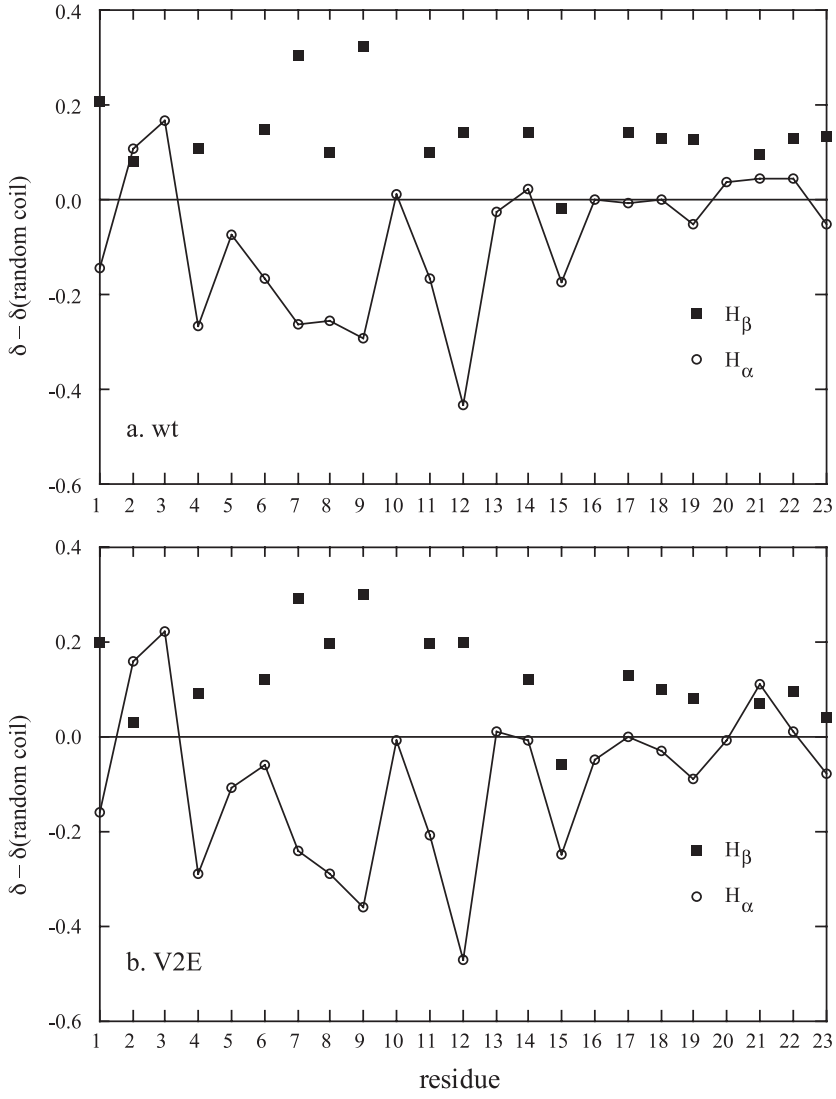

Fig. 2. The CSI for αH (○) and βH (■) for (a) wt FP and (b) the V2E mutant in DPC micelles at 298 K. Negative values represent upfield shifts. The data suggest that the main helical region for both peptides ranges from Ile[4] to Ala[15]. The data at 310 K yields similar patterns for both peptides.

3.3. The V2E mutant

The chemical shifts of the V2E mutant in DPC micelles, assigned in the same fashion as in the wt FP, are given in Table 1b. The intramolecular NOE patterns are similar to that of the wt FP, signifying that there is very little difference in the conformation between the wt FP and the V2E mutant. This is consistent with the MD study of these two FPs as well as other mutants in POPE bilayers conducted in our laboratory [24] which showed that there is little difference in their conformations.

The CSI plots for the V2E FP are also similar to those of the wt FP (Fig. 2), yet another indication that the two FPs share the same conformational characteristics, i.e., an α-helical region spanning from Ile[4] to Leu[12] or from Ile[4] to Ala[15]. In addition, the CSI pattern for both the wt and V2E FPs is very similar to that of Chang et al. for the wt FP in SDS micelles [29]. Thus, the wt FP maintains the same secondary structure in anionic as well as in zwitterionic membrane mimics. The helical region determined in this work is also in agreement with that determined from ^{13}C-enhanced FTIR [52].

The TOCSY spectra of both wt and V2E revealed differences in the conformational flexibilities between the helical (~4–14) segment and the C-terminus. The TOCSY spectra showed strong propagation of the TOCSY correlations for residues in the C-terminal region, e.g., Arg[22] and Met[19] because of the longer T_2 (due to the higher flexibility) in this region. In contrast, for residues in the α-helical region such as Ile[4], Leu[9] and Leu[12], the correlations are much weaker, especially for those longer-range correlations such as NH-βH and NH-γH, because of the shorter T_2 in this region. The difference in the flexibility between these two regions arises from two factors. The α-helical region is more conformationally rigid and the motions of this segment are further restricted from the interactions with the micelle. In

contrast, the C-terminal segment is more conformationally flexibility and does not interact with the micelle to a significant extent (see also Spin label studies). The difference in motional flexibility as revealed by TOCSY spectra has been discussed previously [43] for other peptide–micelle systems.

3.4. Diffusion studies of the binding of the FP to the DPC micelles

The diffusion coefficients of the wt and V2E peptides in water, in DPC micelles and in 4:1 DPC/SDS mixed micelles and the partition coefficients [45] for the peptides in DPC and in mixed micelles are given in Table 2. The diffusion measurements of the pure DPC and the 4:1 DPC/SDS micelles showed that the size of the mixed micelles are only slightly larger than the DPC micelles and that DPC and SDS are homogeneously mixed in the resulting micelles. Thus, the DPC/SDS micelles represent a good mimic for membranes containing both zwitterionic and (~20%) anionic lipids. The partition coefficients for the two peptides in DPC micelles are practically the same within experimental errors. Upon the addition of 20% of the negatively charged SDS surfactants, the partition coefficients for both peptides were found to increase. The increase is ~6-fold for the V2E mutant and ~4-fold for the wt FP. However, the uncertainty for the partition coefficient for V2E in the DPC/SDS mixed micelles is unusually high because the bound fraction of the peptide, f_b, is too close to 1. This is an inherent problem of methods utilizing the ratio of $f_b/(1-f_b)$ to determine the partition coefficient [44,55]. Thus, in both the zwitterionic DPC micelles, and in the anionic/zwitterionic mixed micelles, the difference in the partition coefficient of these two peptides does not correlate with their fusogenic activities, demonstrating that the loss of activity due to the V2E mutation is not due to a decrease in the membrane affinity. Whatever difference in the partition coefficients observed here is actually in the opposite direction of their activities. That is, the partition coefficient of the V2E mutant is actually slightly higher than that of the wt FP in both mimics. This is consistent with observations that different FPs showed similar membrane affinity and yet vastly different activity [10,49]. This means that it is the mode of membrane interaction of the respective FP (discussed in the next section), rather than its membrane affinity, that determines its fusogenic activity.

The significant increases in the partition coefficients of both FPs when anionic lipids are incorporated into the micelles indicate that there must be significant electrostatic interactions of the FP with the negatively charged SDS head groups. The MD simulation of the hydrophobic 16-residue FPs in the zwitterionic POPE bilayer showed that there is virtually no hydrogen-bonding or electrostatic interactions between either the backbone or the side chains of the FP with the micellar surface [24]. The interaction of the FP with the bilayer is primarily via hydrophobic interactions. The situation may be quite different when anionic lipids are present. Previous studies indicated that FP-induced membrane fusion does not occur in zwitterionic phosphatidylcholine (PC) bilayers, and will occur only if negatively charged lipids are present [51]. The substantially increased interactions between the FPs and the lipids in the anionic/zwitterionic micelles observed in this work are the likely cause for the difference in the effects of the FPs in inducing fusion in these two types of bilayers.

3.5. Structures of the FPs from simulated annealing

Fifty structures were generated using the SA protocol for each peptide. For the wt peptide, 15 structures that have the lowest total energy and NOE violation energy converged with a similar global fold. The average total, nonbound, and NOE violation energies of these structures were 315.1±3.6, 140.6±2.2, and 26.0±1.1 kcal mol^{-1}, respectively. No NOE violation greater than 0.2 Å was found in any of these structures. Superimposing the backbone atoms of the segment 3–20 gave a backbone RMSD of 0.23 Å for this region, while the mean global backbone RMSD was 0.33±0.10 Å. The average dihedral angles for the 15 structures are shown in Table 3a. For the V2E peptide, 20 structures that have the lowest total energy and NOE violation energy converged with a similar global fold. The average total, nonbound, and NOE violation energies of these structures were 289.8±6.6, 137.5±2.7, and 29.1±1.8 kcal mol^{-1}, respectively. No NOE violation greater than 0.2 Å was found in any of these structures. Superimposing the backbone atoms of the segment 3–19 gave a backbone

Table 2
The diffusion coefficients (in 10^{-11} m^2 s^{-1})[a] and the partition coefficients, K_p, of the wt FP and the V2E mutant in DPC and in 4:1 DPC/SDS micelles

System	D_{obs}	D_b	D_{free}	f_b	K_p (M^{-1})
wt FP in DPC	7.0±0.1	5.7±0.1	18.0±0.1	0.89±0.01	7.2±0.7×10^3
wt FP in DPC/SDS	5.6±0.1	5.3±0.1	18.0±0.1	0.98±0.01	2.9±0.9×10^4
V2E in DPC	8.2±0.2	7.5±0.2	17.7±0.1	0.93±0.03	1.1±0.4×10^4
V2E in DPC/SDS	6.2±0.1	6.1±0.1	17.7±0.1	0.99±0.01	6.7±2.9×10^4*

[a] Diffusion coefficients were determined from the averages of several peaks in the spectrum, and, with the exception of V2E in DPC, from duplicate measurements of the same samples.

* The large uncertainty is due to the high f_b value. This problem has been discussed by Thorgeirsson, et al. [55] and by Wong and Gao [44].

Table 3a
Average dihedral angles for the wt FP

Residue	ϕ	ψ
Ala^{1}		36.1±79.9
Val^{2}	−63.5±34.6	91.0±54.5
Gly^{3}	166.7±72.7	−58.0±10.8
Ile^{4}	−69.0±3.8	−48.6±4.1
Gly^{5}	−70.6±4.1	1.5±8.8
Ala^{6}	−101.1±8.8	−51.7±1.4
Leu^{7}	−60.8±4.1	−43.2±4.1
Phe^{8}	−63.1±3.1	−35.3±2.1
Leu^{9}	−64.9±4.1	−34.5±4.1
Gly^{10}	−71.9±4.1	−47.7±2.1
Phe^{11}	−62.8±3.9	−52.6±4.1
Leu^{12}	−66.8±4.1	−28.1±4.1
Gly^{13}	−64.3±4.1	−39.6±0.9
Ala^{14}	−70.3±4.1	−46.0±4.1
Ala^{15}	−61.9±4.1	−34.8±4.1
Gly^{16}	−69.2±2.7	−33.8±3.1
Ser^{17}	−74.2±4.1	−36.7±4.2
Thr^{18}	−69.0±4.1	−42.6±4.6
Met^{19}	−66.2±4.1	−36.6±4.1
Gly^{20}	−138.2±5.2	64.2±8.2
Ala^{21}	−74.3±7.0	68.2±40.7
Arg^{22}	−95.8±23.4	108.0±51.5
Ser^{23}	−73.5±38.8	65.0±49.5

RMSD of 0.28 Å for this region, while the mean global backbone RMSD was 0.41±0.13 Å. The average dihedral angles for the 20 structures are shown in Table 3b.

From the SA simulation results, wt peptide adopts a well-defined α helical conformation from Ile^{4} to Met^{19}. As shown in Table 3a, the dihedral angles in this region are close to the ideal α-helical values of -57° and -47° for ϕ and ψ, respectively. The N-terminal segment Ala^{1}–Val^{2}–Gly^{3} and the C-terminal residue Ser^{23} remain flexible. The segment Gly^{20}–Ala^{21}–Arg^{22}, though also quite flexible, exhibits a sheet-like extended structure, which bends (at Gly^{20}) away from the helix axis with an angle of 60–90°.

V2E peptide also adopts an α helical conformation from Ile^{4} to Met^{19}. A well-defined α helix was formed in the region from Ile^{4} to Gly^{16} in all the 20 structures being analyzed. The dihedral angle ϕ and ψ for these residues are close to the ideal α-helical values. The α helical conformation in the region from Ser^{17} to Met^{19} is less well defined, as most (11 out of 20) of the analyzed structures exhibits an α helical conformation from Ile^{4} to Met^{19} or farther (Gly^{20} or Ala^{21}) while the rest of the structures exhibits either a 3_{10} helix or a twist turn in the region Ser^{17}–Met^{19}. The N-terminus Ala^{1}–Val^{2}–Gly^{3} remains flexible. The C-terminal Gly^{20}–Ser^{23} is also flexible, however, there is a tendency for this region to maintain a helical feature.

The conformations determined by SA simulation for the wt and V2E peptides are very similar. Both peptides adopt an α helical conformation in the region from Ile^{4} to Met^{19}. There is a difference in the C-terminus. The C-terminus of wt has an extended conformation and bends away from the helix axis of the peptide, while the C-terminus of V2E has a tendency to maintain a helical conformation along the helix axis of the peptide. However, this difference may become less important due to the flexibility of the C-terminus.

There is a trend revealed in Tables 3a and 3b for the α helical residues of both peptides: more negative ϕ values than ideal and less negative ψ than ideal were found for most of the α helical residues. This is often observed in helical regions in proteins, as carbonyl oxygen atoms of the helical residues are in a position that allows them to be hydrogen bonded to the corresponding amide hydrogen atom in the helix as well as to be able to form hydrogen bonds with solvent water molecules [56].

3.6. Spin label studies

3.6.1. The wt FP

The effects of the spin labels (SL) 5-DS and 16-DS on the peptides were mainly examined from the TOCSY spectra of the FPs, although the NOESY spectra were also examined in most cases to provide corroborative information. In Fig. 3, the NH-side chain proton region of the TOCSY spectra of the wt FP in DPC micelles in the absence and in the presence of SL 5-DS and 16-DS, respectively, is shown. The unpaired electron in the spin labels induces paramagnetic relaxation and selectively broadens the NH resonances of the residues in close spatial proximity to the spin label, reducing the intensities of the affected resonance, and, in some cases, practically eliminating the TOCSY signals arising from that affected residue. The distribution of the nitroxide radical of 5-DS is from the lipid head groups to approximately the C_3

Table 3b
Average dihedral angles for the V2E mutant

Residue	ϕ	ψ
Ala^{1}		40.6±61.8
Glu^{2}	−36.2±78.0	−5.2±40.0
Gly^{3}	−160.4±11.6	−49.5±36.4
Ile^{4}	−52.7±42.8	−38.5±5.9
Gly^{5}	−60.0±3.0	−37.1±2.6
Ala^{6}	−70.8±3.0	−44.2±3.0
Leu^{7}	−64.4±1.9	−42.7±1.6
Phe^{8}	−69.2±1.6	−30.8±3.0
Leu^{9}	−69.6±3.0	−38.8±3.0
Gly^{10}	−64.8±3.0	−34.5±1.4
Phe^{11}	−70.1±3.5	−56.8±2.2
Leu^{12}	−63.7±2.1	−39.8±2.9
Gly^{13}	−62.3±2.0	−36.5±1.7
Ala^{14}	−75.4±1.5	−45.9±3.1
Ala^{15}	−60.2±2.3	−36.9±3.1
Gly^{16}	−68.9±3.1	−32.0±4.1
Ser^{17}	−74.4±5.4	−14.6±30.5
Thr^{18}	−97.0±38.1	−56.5±3.2
Met^{19}	−72.3±9.4	36.6±52.1
Gly^{20}	−167.2±13.5	−31.8±20.0
Ala^{21}	−41.2±61.8	−21.2±29.8
Arg^{22}	−80.3±56.2	−14.0±46.2
Ser^{23}	−104.0±32.6	59.8±51.8

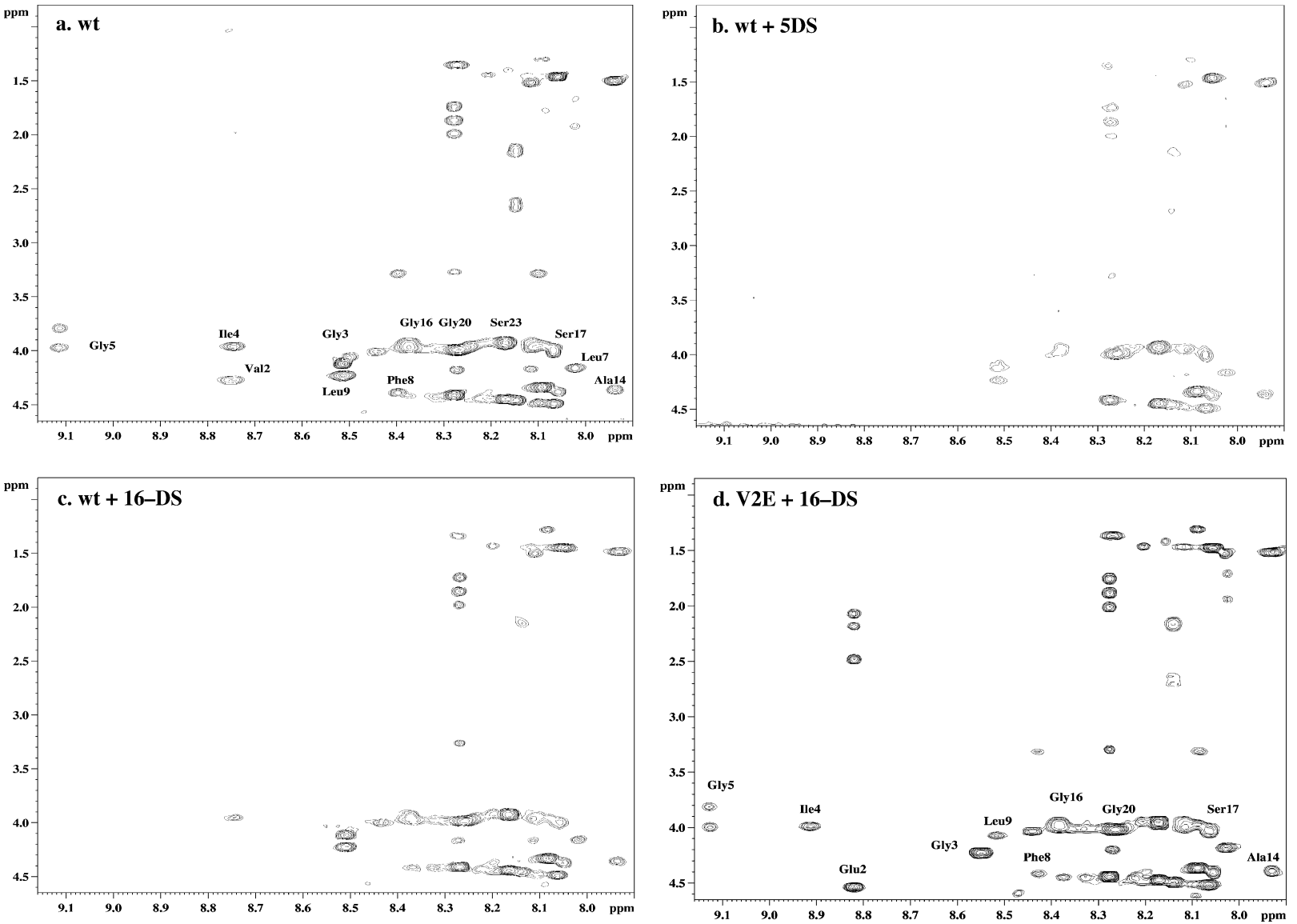

Fig. 3. The effects of SL 5-DS and 16-DS on the TOCSY spectra of the wt FP and the V2E mutant in DPC micelles at 310 K. (a) wt FP without SL; (b) wt FP in the presence of 5-DS. Note the disappearance of the NH signals of Val^2, Ile^4, Gly^5 and Phe^8; (c) wt FP in the presence of 16-DS; (d) V2E mutant in the presence of 16-DS. It is evident that 16-DS has virtually no effect on any of the NH signals of V2E with the exception of a minor attenuation of the Phe^8 signals.

Table 4
The degree of attenuation of the NH signals in the TOCSY spectra of the wt 23-mer FP in 90 mM DPC micelles by spin-labels 5-DS and 16-DS

Residue	wt+5-DS	wt+16-DS	V2E+5-DS	V2E+16-DS
Val2/Glu2	vl	vl	vl	no
Gly3	l	s	s	no
Ile4	vl	m	vl	no
Gly5	vl	vl	vl	no
Ala6	l	s	s	no
Leu7	m	m	s	no
Phe8	vl	m	l	s
Leu9	m	s	l	no
Gly10	m	m	m	no
Phe11	m	s	s	no
Leu12	s	s	m	no
Gly13	s	s	m	no
Ala14	s	s	s	no
Ala15	m	s	m	no
Gly16	s	s	m	no
Ser17	s	no	no	no
Thr18	no	no	no	no
Met19	no	no	no	no
Gly20	no	no	no	no
Ala21	no	no	no	no
Arg22	no	no	no	no
Ser23	no	no	no	no

vl, *l*, *m*, *s* and *no* denote very large (>80%); large (50–80%); medium (20–50%); small (<20%); and no (no detectable effects), respectively.

position in the lipid chain [29], and the location in 16-DS is near the end of the alkyl chain and close to the center of the micelles, as shown by ^{13}C line-broadening of the micellar lipid hydrocarbon chains in Refs [57,58], and in this work (data not shown). Combining the application of these two spin-labels can facilitate locating the residue with respect to the membrane/water interface [57–60]. For the wt type FP, by comparing the TOCSY spectra in the absence (Fig. 3a) and presence of SL 5-DS (Fig. 3b), it is immediately evident that the effects of the SL on the NH signals are the strongest at the N-terminal and diminish gradually going towards the C-terminus. For example, in Fig. 3b, the NH signals of Val^2, Ile^4 and Gly^5 practically disappeared. On the other hand, the NH signals of residues from Thr^{18} to Ser^{23} were hardly attenuated. The attenuation of the signals corresponding to residues from Leu^9 to Ser^{17} falls in between these two extremes. The only exception to this monotonic trend is the large attenuation of the Phe^8 signal, which also essentially disappeared (Fig. 3b). The lack of effects of 5-DS, which has its unpaired electron close to the surface of the micelles, on the signals of residues 18–23 indicates that these C-terminal residues are not associated with the micellar surface, but are protruding into the aqueous phase. This situation is quite similar to the results of our study on ACTH (1–24) in DPC micelles, where the polar C-terminal segment was found to be primarily in the aqueous solution with very little association with the micelles [43]. The degree of attenuation for the signals from various residues is summarized in Table 4.

Qualitatively, the pattern of attenuation in the 16-DS (Fig. 3c) is similar to that as in 5-DS, i.e., the degree of attenuation is the strongest at the N-terminal region and gradually diminishes moving towards the C-terminus. Quantitatively, the attenuation is uniformly lower than in the 5-DS sample. However, even in the 16-DS sample, the signals arising from Val^2 and Gly^5 were found to have virtually disappeared, and the attenuation is significant for Ile^4 and Phe^8. Since the distribution of the nitroxide radical of 5-DS is near the lipid head groups, and the location in 16-DS is near the end of the alkyl chain at the center of the micelles, the effects of 16-DS must imply that part of the N-terminus is inside of the head group region in the micellar interior. Thus, the combined results of the 5-DS and 16-DS clearly showed that the N-terminus of the wt FP inserts partially into the interior of the micelles.

The spin label results for the wt FP in the present study are consistent with the N-terminal insertion model [17,18,24,25], but in contrast with the results of Chang et al. [29] for the wt FP in SDS micelles which appeared to show that the Leu^7-Phe^8 segment is inserted deeply into the micellar core while both the N- and C-termini reside on the surface of the micelles. Our results showed that Phe^8 is much more attenuated by 5-DS than by 16-DS

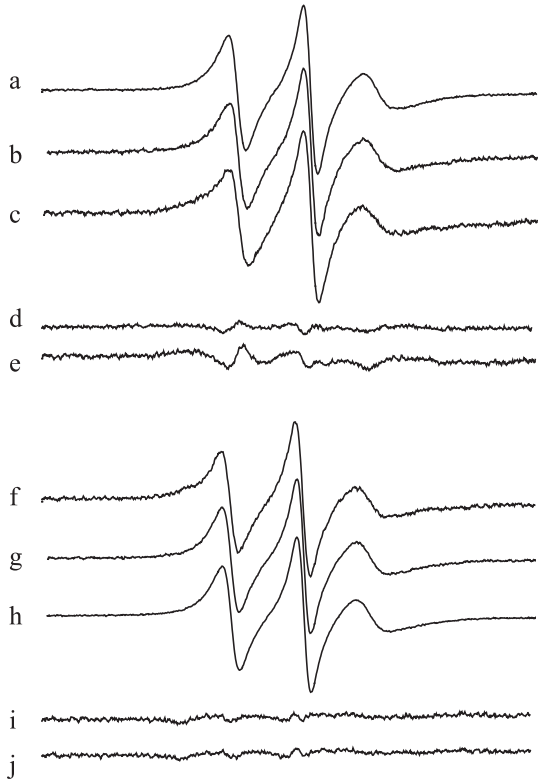

Fig. 4. ESR spectra of the SL 5-DS in DPC micelles in the absence and presence of different concentrations of the wt and V2E FPs. The spectra, taken at room temperature, showed no line-broadening upon the addition of the FP. Nor was there any broad component in the difference spectra. (a) no wt FP; (b) 0.5 mg wt FP; (c) 1.0 mg wt FP; (d) b–a; (e) c–a; (f) no V2E; (g) 0.5 mg V2E; (h) 1.0 mg V2E; (i) g–f; (j) h–f.

(Fig. 3b and c), and the signal of Leu[7] is only modestly attenuated in both cases, discounting the model of deep immersion of the Leu[7]-Phe[8] segment in the DPC micelles. According to our MD simulations [24], there is a slight bent of the N-terminal segment (approximately Ala[1]–Val[2]) towards the interface of the membrane to enable the protonated amino N-terminus to be close to the interface and to interact with the head groups resulting in a stabilization of this configuration [19,20]. However, no large-scale bend, or the immersion of the Leu[7]-Phe[8] segment into the micellar interior as suggested by Chang et al. [29], was indicated in the present data.

3.6.2. The V2E Mutant

For the V2E mutant, the effects of the addition of 5-DS to the DPC sample are similar to, but less in magnitude than, the wt case. The NH signals of Ile[4] and Gly[5] in the TOCSY spectra were found to be highly, but not completely, attenuated. In addition, the signals of Phe[8] were also significantly attenuated (figure not shown). The signals of

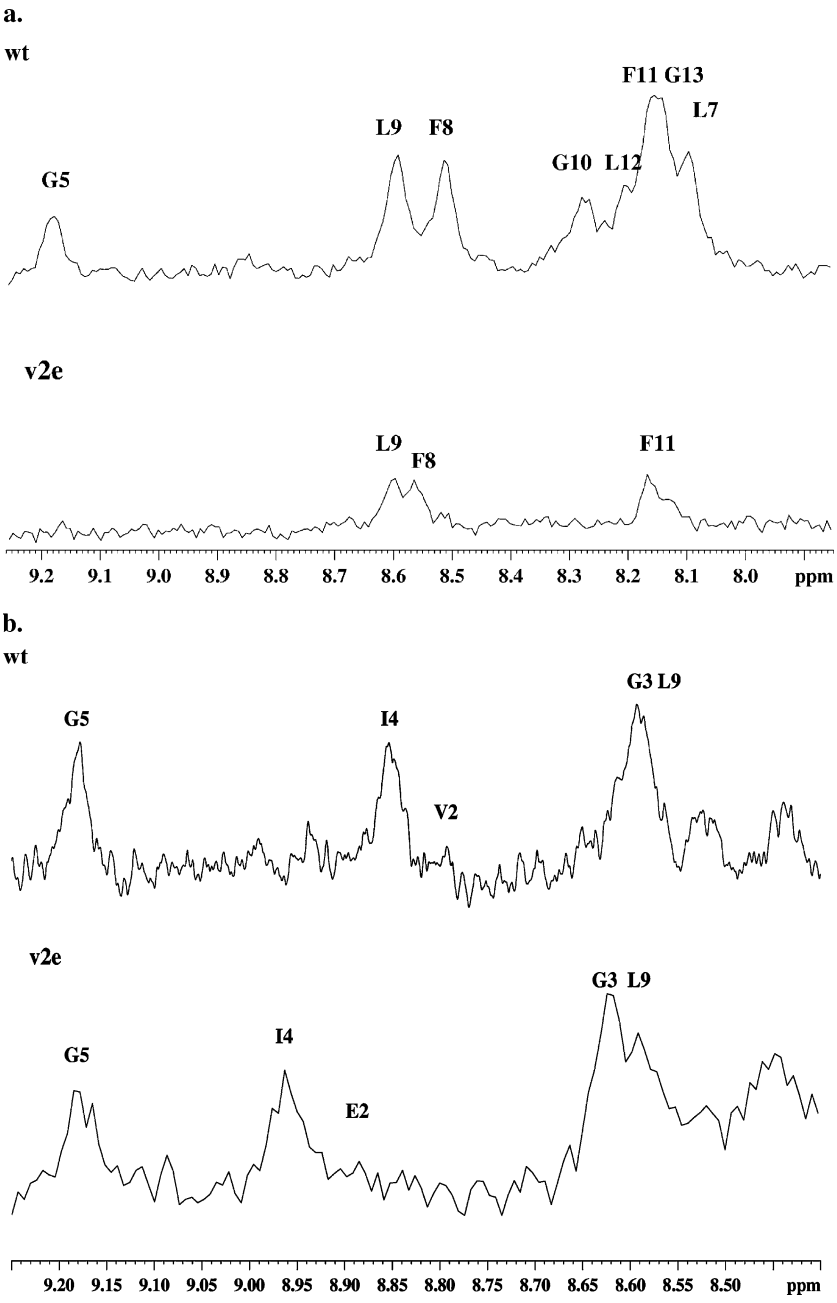

Fig. 5. (a) The 1D spectra of the amide proton region of the wt (top) and V2E (bottom) samples in DPC (at 293 K) after >30 min of exchange with D_2O. Sixty four-scans were taken for each of these spectra. (b) The 1D spectra of the amide proton region of the wt (top) and V2E (bottom) samples in DPC (at 293 K) after 5 min of exchange with D_2O. Note the rapid disappearance of the signals of the protons at Val[2] (in wt) and Glu[2] (in V2E). Four scans were taken for each of these spectra.

Ala[6] and Leu[7] were too overlapped to make a clear judgment on the attenuation of the individual signals. The degree of attenuation decreases towards the C-terminus as in the wt case. Again, as in the wt case, the signals of Thr[18]-Ser[23] are not attenuated by 5-DS, indicating that this C-terminal segment is not in association with the micellar surface. The most contrasting results for V2E from those of the wt FP came from the 16-DS sample. No noticeable attenuation of any NH signals was observed throughout the peptide (Fig. 3d) upon the addition of 16-DS, with the exception of a small attenuation of the signal of Phe[8]. Since the nitroxide free radical in 16-DS locates in the interior of and close to the center of the DPC micelles, the complete lack of its effects on the signals of any residue in V2E and the difference from the wt case offer strong indications that V2E binds to the DPC micelles on the micellar surface, and does not insert into the micellar interior, different from that of the wt FP. This result is in excellent correspondence with the results of the MD simulation study from this laboratory, which showed that wt inserts into the POPE bilayer obliquely at ~44±6° while V2E binds on the surface of the bilayer [24].

3.7. ESR of spin-labels

There was a report in the literature that the spin-labels DS may form complexes with the FP in zwitterionic vesicles [31], thus rendering the spin-label results ambiguous. To determine whether FP–SL complex formation takes place in our samples, ESR spectra were taken of the SL in DPC micelles in concentrations similar to those in NMR experiments. Three samples of each FP (wt or V2E) were thus tested: no FP, 0.5 mg FP (~1.2 mM) and 1 mg FP (~2.4 mM), respectively. The FP concentrations are also similar to those used in the NMR experiments. In each case, there was no detectable change in the ESR spectra when FP was introduced into the sample (Fig. 4). Subtraction of the spectrum from the sample without FP from spectra containing FP revealed no broad spectral component, or "motionally-restricted component" as suggested by Curtain et al. [31]. Thus, we can conclude that at the concentrations of FP and SL pertinent to the NMR studies, there was no FP–SL complex formation and the SL results can reliably be used to provide locational information of the peptide with respect to the micelles.

3.8. Deuterium amide–proton exchange

Amide proton–deuterium exchange results showed considerable difference between the wt and the V2E samples. After about ~15 min of exchange, the NH signals of the V2E sample practically disappeared (Fig. 5a). Only very weak signals remained for the most hydrophobic residues F8, L9 and F11. In contrast, substantially larger residual signals from residues G5–G13 were observed for the wt FP. This observed difference is consistent with the model from the MD studies [24] and from the spin-label results in this work. That is, the wt FP inserts its N-terminus into the membrane interior while the V2E mutant lies on the surface of the membrane. The first two residues near the protonated N-terminus in the wt FP are actually turned towards and in close proximity to the water–membrane interface, as the early spectra (taken in the first 5–10 min) in the deuterium exchange showed that the amide protons of V2 in the wt FP and E2 in V2E were the first to be exchanged away (Fig. 5b). This is in agreement with the conclusion of our MD work [24] and some previous work on influenza HA-2 FP as well [19,20], and consistent with the expectation that the protonated N-terminus does not prefer to be in contact with the hydrophobic interior of the membrane. This is one of the major reasons for the oblique (rather than perpendicular) insertion of the active FPs.

The Monte-Carlo simulation of Maddox and Longo of the wt and V2E FPs in a bilayer [26] showed that, while the wt FP is primarily in the inserted form, the lowest energy conformation for the V2E mutant is the trans-membrane form. Our present results from the spin-labeled and deuterium amide exchange experiments are not in agreement with their results, but are, on the other hand, perfectly consistent with the MD simulation results obtained from our laboratory [24].

4. Conclusions

In this work, a number of NMR techniques were used to determine the structure, the membrane affinity and the mode of binding to membrane mimics for two fusion peptides of the HIV fusion protein gp41, the active wt 23-residue FP and the V2E mutant. The main conclusions reached from this study are summarized as follows.

(1) The activities of the FP are not correlated with the membrane affinities of these peptides based on the PFG diffusion data in DPC and in 4:1 DPC/SDS mixed micelles. The V2E was actually found to have marginally higher affinity for the membrane mimicking micelles than the active wt FP, opposite in direction of their respective activities. When combined with Conclusion 3 (below), it is clear that it is the mode of binding of the FP to the membrane that is critical to the fusogenic activity of the FP, rather than its membrane affinity.

(2) The secondary structures of these two FPs are practically identical. Based on the NOE and secondary chemical shifts, the structures of both FPs are characterized by an α-helical segment spanning the region from Ile[4] to Leu[12] or to Ala[15]. The C-terminal segment consists of mixtures of 3_{10} and/or nascent helices. Simulated annealing showed that the helical region extends from Ile[4] to Met[19]. The similarity in the secondary structures of wt and V2E despite their vastly different activities suggests that the conformation of the FP is not a major parameter in determining the activity of the FP. Conformational flexibility, however, has been shown in an MD simulation in our

laboratory [27] to be a significant factor that differentiates active and inactive FPs. Conformational flexibility of these two FPs has not been closed examined in the present study.

(3) The spin-label and deuterium amide exchange studies provided convincing evidence that showed significant differences between the modes of binding of these two peptides with the DPC micelles. The results for the wt FP from the spin-labels 5-DS and 16-DS suggest a N-terminal insertion model. However, for the V2E mutant, the NMR signals are completely unaffected by the SL 16-DS which has its unpaired electron located in the interior of the micelle, indicating that the peptide is not inserted into the micelle at all. This conclusion is in excellent agreement with our MD simulation studies of these two FPs in a POPE bilayer [24], and with the hypothesis that the activity of the gp41 FP is predicated on an oblique insertion of the FP into the membrane based on several previous experimental studies [17,18,25].

Furthermore, the results of this work are in excellent agreement with those of our MD simulation of these two, and other, FPs in membrane mimics [24]. The agreement is particularly encouraging in demonstrating that simulation and experimental approaches can be applied synergistically to obtain more definite and detailed structural and dynamical properties of these systems and to provide interpretations of molecular events that may not be clear based on experiment or simulations alone. Although micelles were used in this work as the membrane mimic while the MD and other previous studies were carried out in bilayers, our MD work on other peptides in DPC micelles and bilayers [61] and the work of Han et al. [21] on the influenza hemagglutinin HA_2 FP showed that the results in DPC micelles and in bilayers are consistent with each other and can thus be directly compared.

Acknowledgments

This work is supported by the Petroleum Research Fund (35495-AC7 and 35495-AC7-SF02), administered by the American Chemical Society, and by the University of Missouri Research Board. The NMR spectrometers were partially funded by grants from the National Science Foundation (CHE-89-08304 and DBI-00-70359). We thank Dr. Fabio Gallazzi of University of Missouri for synthesizing the fusion peptides for this study, and David Dye of the Department of Chemistry, Indiana University for his help in measuring the ESR spectra.

References

[1] F.D. Veronese, A.L. DeVico, T.D. Copeland, S. Oroszlan, R.C. Gallo, M.G. Sarngadharan, Characterization of gp41 as the transmembrane protein coded by the HTLV/LAV envelope gene, Science 229 (1985) 1402–1405.

[2] D.C. Chan, D. Fass, J.M. Berger, P.S. Kim, Core structure of gp41 from the HIV envelope glycoprotein, Cell 89 (1997) 263–273.

[3] S.G. Peisajovich, R.F. Epand, M. Pritsker, Y. Shai, R.M. Epand, The polar region consecutive to the HIV fusion peptide participates in membrane fusion, Biochemistry 39 (2000) 1826–1833.

[4] A.L. Lasky, G. Nakamura, D.H. Smith, C. Fennie, C. Shimasaki, E. Patzer, P. Berman, T. Gregory, D.J. Capon, Delineation of a region of the human immunodeficiency virus type 1 gp120 glycoprotein critical for interaction with the CD4 receptor, Cell 50 (1987) 975–985.

[5] H.M. Choe, M. Farzan, Y. Sun, N. Sullivan, B. Rollins, P.D. Ponath, L.J. Wu, C.R. Mackay, G. LaRosa, W. Newman, N. Gerard, C. Gerard, J. Sodroski, The beta-chemokine receptors CCR3 and CCR5 facilitate infection by primary HIV-1 isolates, Cell 85 (1996) 1135–1148.

[6] B.J. Doranz, J. Rucker, Y.J. Yi, R.J. Smyth, M. Samson, S.C. Peiper, M. Parmentier, R.G. Collman, R.W. Doms, A dual-tropic primary HIV-1 isolate that uses fusin and the beta-chemokine receptors CKR-5, CKR-3, and CKR-2b as fusion cofactors, Cell 85 (1996) 1149–1158.

[7] T. Dragic, V. Litwin, G.P. Allaway, S.R. Martin, Y.X. Huang, K.A. Nagashima, C. Cayanan, P.J. Maddon, R.A. Koup, J.P. Moore, W.A. Paxton, HIV-1 entry into CD4(+) cells is mediated by the chemokine receptor CC-CKR-5, Nature 381 (1996) 667–673.

[8] M. Kowalski, J. Potz, L. Basiripour, T. Dorfman, W.C. Goh, E. Terweilliger, A. Dayton, C. Rosen, W. Haseltine, J. Sodroski, Functional regions of the envelope glycoprotein of human immunodeficiency virus type 1, Science 237 (1987) 1351–1355.

[9] W.H. Gallaher, Detection of a fusion peptide sequence in the transmembrane protein of human immunodeficiency virus, Cell 50 (1987) 327–328.

[10] M. Pritsker, J. Rucker, T.L. Hoffman, R.W. Doms, Y. Shai, Effect of nonpolar substitutions of the conserved Phe11 in the fusion peptide of HIV-1 gp41 on its function, structure, and organization in membranes, Biochemistry 38 (1999) 11359–11371.

[11] E.O. Freed, D.J. Myers, R. Risser, Characterization of the fusion domain of the human immunodeficiency virus type 1 envelope glycoprotein gp41, Proc. Natl. Acad. Sci. U. S. A. 87 (1990) 4650–4654.

[12] E.O. Freed, E.L. Delwart, G.L. Buchschacher, A.T. Panganiban, A mutation in the human immunodeficiency virus type 1 transmembrane glycoprotein gp41 dominantly interferes with fusion and infectivity, Proc. Natl. Acad. Sci. U. S. A. 89 (1992) 70–74.

[13] M.D. Delahunty, I. Rhee, E.O. Freed, J.S. Bonifacino, Mutational analysis of the fusion peptide of the human immunodeficiency virus type 1: Identification of critical glycine residues, Virology 218 (1996) 94–102.

[14] P.W. Mobley, A.J. Waring, M.A. Sherman, L.M. Gordon, Membrane interactions of the synthetic N-terminal peptide of HIV-1 gp41 and its structural analogues, Biochim. Biophys. Acta 1418 (1999) 1–18.

[15] F.B. Pereira, F.M. Goni, J.L. Nieva, Liposome destabilization induced by the HIV-1 fusion peptide: effect of a single amino acid substitution, FEBS Lett. 362 (1995) 243–246.

[16] F.B. Pereira, F.M. Goni, J.L. Nieva, Permeabilization and fusion of uncharged lipid vesicles induced by the HIV-1 fusion peptide adopting an extended conformation: dose and sequence effects, Biophys. J. 73 (1997) 1977–1986.

[17] I. Martin, F. Defrise-Quertain, E. Decroly, M. Vandenbranden, R. Brasseur, J.M. Ruysschaert, Orientation and structure of the NH2-terminal HIV-1 gp41 peptide in fused and aggregated liposomes, Biochim. Biophys. Acta 1145 (1993) 124–133.

[18] I. Martin, H. Schaal, A. Scheid, J.M. Ruysschaert, Lipid membrane fusion induced by the human immunodeficiency virus type 1 gp41 N-terminal extremity is determined by its orientation in the lipid bilayer, J. Virol. 70 (1996) 298–304.

[19] Z. Zhou, J.C. Makosko, D.W. Hughes, B.G. Sayer, J. Hawes, R.M. Epand, ^{15}N NMR study of the ionization properties of the influenza virus fusion peptide in zwitterionic phospholipid dispersions, Biophys. J. 78 (2000) 2418–2425.

[20] J.C. Macosko, C.H. Kim, Y.K. Shin, The membrane topology of the fusion peptide region of influenza hemagglutinin determined by spin-labeling EPR, J. Mol. Biol. 267 (1997) 1139–1148.
[21] X. Han, J. Bushweller, D. Cafiso, L.K. Tamm, Membrane structure and fusion-triggering conformational change of the fusion domain from influenza hemagglutinin, Nat. Struct. Biol. 8 (2001) 715–720.
[22] R. Brasseur, M. Vanderbranden, B. Cornet, A. Burny, J.M. Ruysschaert, Orientation into the lipid bilayer of an asymmetric amphipathic helical peptide located at the N-terminus of viral fusion proteins, Biochim. Biophys. Acta 1029 (1990) 267–273.
[23] J. Nieva, S. Nir, A. Muga, F.M. Goni, J. Wilschut, Interaction of the HIV-1 fusion peptide with phospholipid vesicles: different structural requirements for fusion and leakage, Biochemistry 33 (1994) 3201–3209.
[24] S.A. Kamath, T.C. Wong, Membrane structure of the human immunodeficiency virus gp41 fusion domain by molecular dynamics simulation, Biophys. J. 83 (2002) 135–143.
[25] J.P. Bradshaw, M.J.M. Darkes, T.A. Harroun, J. Katsaras, R.M. Epand, Oblique membrane insertion of viral fusion peptide probed by neutron diffraction, Biochemistry 39 (2000) 6581–6585.
[26] M.W. Maddox, M.L. Longo, Conformational partitioning of the fusion peptide of HIV-1 gp41 and its structural analogs in bilayer membranes, Biophys. J. 83 (2002) 3088–3096.
[27] T.C. Wong, Membrane structure of the human immunodeficiency virus gp41 fusion peptide by molecular dynamics simulation: II. The glycine mutants, Biochim. Biophys. Acta, Biomembr. 1609 (2003) 45–54.
[28] G. Myers, B. Korber, J.A. Berzofsky, R.F. Smith, G.N. Pavalakis, Human Retroviruses and AIDS 1991: A Compilation and Analysis of Nucleic Acid and Amino Acid Sequences, Los Alamos National Laboratory, Los Alamos, 1991.
[29] D.K. Chang, S.F. Cheng, W.J. Chien, The amino-terminal fusion domain peptide of human immunodeficiency virus type 1 gp41 inserts into the sodium dodecylsulfate micelle primarily as a helix with a conserved glycine at the micelle-water interface, J. Virol. 71 (1997) 6593–6602.
[30] P.L. Vidal, L. Chalon, A. Heitz, N. Van Mau, J. Mery, G. Divita, F. Heitz, Interactions of primary amphipathic vector peptides with membranes. Conformational consequences on cellular localization, J. Membr. Biol. 162 (1998) 259–264.
[31] C. Curtain, F. Separovic, K. Nielson, D. Craik, Y. Zhong, A. Kirkpatrick, The Interactions of the N-terminal fusogenic peptide of HIV-1 gp41 with neutral phospholipids, Eur. Biophys. J. 28 (1999) 427–436.
[32] J. Yang, P.D. Parkanzk, B.A. Khunte, C.G. Canlas, R. Yang, C.M. Gabrys, D.P. Weliky, Solid state NMR measurements of conformation and conformational distributions in the membrane-bound HIV-1 fusion peptide, J. Mol. Graph. Model. 19 (2001) 129–135.
[33] J. Yang, C.M. Gabrys, D.P. Weliky, Solid state nuclear magnetic resonance evidence for an extended β strand conformation of the membrane-bound HIV-1 fusion peptide, Biochemistry 40 (2001) 8126–8137.
[34] R. Yang, J. Yang, D.P. Weliky, Synthesis, enhanced fusogenicity, and solid state NMR measurements of cross-linked HIV-1 fusion peptides, Biochemistry 42 (2003) 3527–3535.
[35] J. Lauterwein, C. Bosch, L.R. Brown, K. Wuthrich, Physico-chemical studies of the protein-lipid interactions in melitten-containing micelles, Biochim. Biophys. Acta 556 (1979) 244–252.
[36] D.G. Davis, A. Bax, Assignment of complex ^{1}H NMR spectra via two-dimensional homonuclear Hartman–Hahn spectroscopy, J. Am. Chem. Soc. 107 (1985) 2820–2821.
[37] G. Griesinger, G. Ottling, K. Wuthrich, R.R. Ernst, TOCSY for ^{1}H spin system identification in macromolecules, J. Am. Chem. Soc. 110 (1988) 7870–7872.
[38] J. Jeener, B. Meier, P. Bachman, R.R. Ernst, Investigation of exchange processes by two-dimensional NMR spectroscopy, J. Chem. Phys. 71 (1979) 4546–4553.
[39] A. Kumar, R.R. Ernst, K. Wuthrich, A two-dimensional nuclear Overhauser enhancement (2D NOE) experiment for the elucidation of complete proton-proton cross-relaxation networks in biological macromolecules, Biochem. Biophys. Res. Commun. 95 (1980) 1–10.
[40] G. Bodenhausen, H. Kogler, R.R. Ernst, Selection of coherence transfer pathways in NMR pulse experiments, J. Magn. Reson. 58 (1984) 370–388.
[41] V. Sklenar, M. Piotto, R. Leppik, V. Saudek, Gradient-tailored water suppression for ^{1}H-^{15}N HSQC experiments optimized to retain full sensitivity, J. Magn. Reson., Ser. A 102 (1993) 241–245.
[42] S.J. Gibbs, C.S. Johnson, A PFG-NMR experiment for accurate diffusion and flow studies in the presence of Eddy currents, J. Magn. Reson. 93 (1991) 395–401.
[43] X.-F. Gao, T.C. Wong, Studies of the binding and structure of adrenocorticotropin peptides in membrane mimics by NMR spectroscopy and pulsed-field gradient diffusion, Biophys. J. 74 (1998) 1871–1888.
[44] T.C. Wong, X.-F. Gao, The temperature dependence and thermodynamic functions of partitioning of substance P peptides in dodecylphosphocholine micelles, Biopolymers 45 (1998) 395–403.
[45] L.K. Tamm, Membrane insertion and lateral mobility of synthetic amphiphilic signal peptides in lipid model membrane, Biochim. Biophys. Acta 1071 (1991) 123–148.
[46] Discover User Guide, September 1996, Molecular Simulations, San Diego.
[47] K. Wuthrich, NMR of Proteins and Nucleic Acids, John Wiley and Sons, New York, 1986.
[48] M. Nilges, G.M. Clore, A.M. Gronenborn, Determination of three-dimensional structures of proteins from interproton distance data by dynamical simulated annealing from a random array of atoms Circumventing problems associated with folding, FEBS Lett. 239 (1988) 129–136.
[49] Y. Kliger, A. Aharoni, D. Rapaport, P. Jones, R. Blumenthal, Y. Shai, Fusion peptides derived from the HIV type 1 glycoprotein 41 associated within phospholipid membranes and inhibit cell-cell fusion, J. Biol. Chem. 272 (1997) 13496–13505.
[50] L.M. Gordon, C.C. Curtain, Y.C. Zhong, A. Kirkpatrick, P.W. Mobley, A.J. Waring, The amino-terminal peptide of HIV-1 glycoprotein 41 interacts with human erythrocyte membranes: peptide conformation, orientation and aggregation, Biochim. Biophys. Acta 1139 (1992) 257–272.
[51] M. Rafalski, J.D. Lear, W.F. DeGrado, Phospholipid interactions of synthetic peptides representing the N-terminus of HIV gp41, Biochemistry 29 (1990) 7917–7922.
[52] L.M. Gordon, P.W. Mobley, R. Pilpa, M.A. Sherman, A.J. Waring, Conformational mapping of the N-terminal peptide of the HIV-1 gp41 in membrane environments using ^{13}C-enhanced Fourier transform infrared spectroscopy, Biochimica 1559 (2002) 96–120.
[53] H.J. Dyson, M. Rance, R.A. Houghten, R.A. Lerner, P.E. Wright, Folding of immunogenic peptide fragments of proteins in water solution, J. Mol. Biol. 201 (1988) 166–200.
[54] D.S. Wishart, B.D. Sykes, F.M. Richards, The chemical shift index: a fast and simple method for the assignment of protein secondary structure through NMR spectroscopy, Biochemistry 31 (1992) 1647–1651.
[55] T.E. Torgeirsson, C.J. Russell, D.S. King, Y.K. Shin, Direct determination of the membrane affinities of individual amino acids, Biochemistry 179 (1996) 131–137.
[56] T.E. Creighton, Protein: Structures and Molecular Properties, W.H. Freeman, New York, 1993.
[57] L.R. Brown, C. Bosch, K. Wuthrich, Location and orientation relative to the micellar surface for glucagon in mixed micelles with dodecylphosphocholine, Biochim. Biophys. Acta 642 (1981) 296–312.
[58] H.W. Van den Hooven, C.A.E.M. Sprink, M. Van de Kamp, R.N.H. Konings, C.W. Hilbers, F.J.M. Van de Ven, Surface location and orientation of the lanbiotic nisin bound to membrane-mimicking

micelles of dodecylphosphocholine and of sodium dodecylsulfate, Eur. J. Biochem. 235 (1996) 394–403.
[59] C.H.M. Papavoine, R.N.H. Konings, C.W. Hilbers, F.J.M. van den Ven, Location of M13 coat protein in sodium dodecyl sulfate micelles as determined by NMR, Biochemistry 33 (1994) 12990–12997.
[60] K. Mattila, R. Kinder, B. Bechinger, The alignment of a voltage-sensing peptide in dodecylphosphocholine micelles and in oriented lipid bilayers by nuclear magnetic resonance and molecular modeling, Biophys. J. 77 (1999) 2102–2113.
[61] T.C. Wong, S. Kamath, Molecular dynamics simulations of adrenocorticotropin (1–24) in a solvated dodecylphosphocholine (DPC) Micelle and in a dimyristoyl-phosphatidylcholine (DMPC) Bilayer, J. Biomol. Struct. Dyn. 20 (2002) 39–57.